



Impact-induced compositional variations on Mercury



Edgard G. Rivera-Valentin^{a,b,*}, Amy C. Barr^{a,b}

^a Brown University, Department of Geological Sciences, 324 Brook St., Box 1846, Providence, RI 02912, United States

^b Center for Lunar Origin and Evolution, Southwest Research Institute, Boulder, CO 80302, United States

ARTICLE INFO

Article history:

Received 11 January 2013

Received in revised form 16 January 2014

Accepted 2 February 2014

Available online xxxx

Editor: C. Sotin

Keywords:

Mercury
impacts
surface composition

ABSTRACT

Remote sensing data suggest Mercury's surface has compositional variations spatially associated with crater and basin ejecta, the so-called "Low-Reflectance Material" (LRM), which has been suggested to be enriched in a subsurface native darkening agent that is excavated and redeposited onto the surface. This unit may record the evidence of impact-induced mixing of Mercury's outer layers during its early history. Here, we develop a fully three-dimensional Monte Carlo model of impact cratering, excavation, and ejecta blanket deposition on a global scale for Mercury.

New dynamical simulations of the early evolution of the asteroid belt hint at the presence of additional asteroids in a region interior to the present-day belt, known as the "E-belt". We use Monte Carlo methods to show that the predicted bombardment from this population matches the observed spatial crater densities on Mercury. Impacts large enough to pierce through the crust create surface ejecta deposits rich in mantle material. Later impacts onto enriched ejecta deposits redistribute mantle material away from the basins. For the suggested average mercurian crustal thickness of 50 km, the surface has, on average, ~0.4% mantle material by volume; the most enriched areas have ~30% mantle by volume.

The regional coverage of impact-induced compositional changes is strongly dependent on the thickness to the subsurface source. Because observations indicate LRM covers ~15% of Mercury's surface, our model suggests the darkening agent is ~30 km deep. Considering the current estimated average mercurian crustal thickness of 50 km, this implies the darkening agent is likely located within a chemically distinct lower crust.

© 2014 Elsevier B.V. All rights reserved.

1. Introduction

The MERcury Surface, Space ENvironment, GEOchemistry, and Ranging (MESSENGER) Gamma-Ray Spectrometer (GRS) and X-Ray Spectrometer (XRS) have been used to map the chemical heterogeneity of Mercury's surface and, by correlating with landforms, infer subsurface composition and primordial conditions (Nittler et al., 2011; Evans et al., 2012; Peplowski et al., 2012; Weider et al., 2012). Though much of Mercury's surface has been altered by smooth plains, the majority of which probably have a volcanic origin (Denevi et al., 2013), the chemical heterogeneity of the heavily cratered terrains will likely show signs of impact-induced compositional variations. In particular, there seem to be chemically distinct units primarily associated with cratering features, such as ejecta blankets.

The Low-Reflectance Material (LRM), which covers ~15% of the surface, is primarily found within crater and basin ejecta (Murchie et al., 2008; Robinson et al., 2008; Denevi et al., 2009). Because

immature impact ejecta on Mercury have lower reflectance than their lunar counterparts, there may be a native darkening agent located at depth (Denevi and Robinson, 2008). Thus, LRM, which can reach reflectance values 30% below the global mean (Denevi et al., 2009), is suggested to be caused by an enrichment in a native darkening agent that is excavated during impacts and redistributed within ejecta blankets (Denevi and Robinson, 2008). Although LRM is generally associated with crater ejecta, it is not found within the continuous ejecta blankets of many impact craters, perhaps suggesting the subsurface darkening agent is not uniformly distributed (Denevi et al., 2009).

For planets with thin crusts, such as Mercury, with an estimated crustal thickness ranging between 20 and 80 km (Smith et al., 2012), impact mixing of mantle and crustal materials may be an efficient process in producing surface compositional heterogeneities. The distribution and magnitude of the heterogeneity will be dependent on the number and size of impactors and the crustal thickness. The number and clustering of ages of lunar impact basins suggest the terrestrial planets experienced a period of frequent impacts ~700 million years after the endpoint of planet formation dubbed the "Late Heavy Bombardment" (LHB) (Tera et al., 1974; Hartmann et al., 2000). Recent work seeking to clarify

* Corresponding author.

E-mail address: rivera-valentin@brown.edu (E.G. Rivera-Valentin).

the number of lunar basins and relatively young terrestrial impact spherule beds suggests this bombardment lasted from the endpoint of planet formation to 2 Gya, longer than previously thought (Bottke et al., 2012). In this scenario, the planets are hit by asteroids from the main belt and E-belt, an extinct asteroid population located interior to the present-day belt. The lunar cratering production function closely matches an E-belt dominated bombardment (Bottke et al., 2012). Because Mercury is an airless inner Solar System body, the evidence of an E-belt dominated bombardment should be recorded on Mercury's ancient, heavily cratered terrain.

Here, we show that this bombardment may be the cause for the suggested impact-induced compositional variations on Mercury. We construct a 3-D Monte Carlo model of impact cratering and ejecta deposition to investigate the effect of an E-belt dominated bombardment on the composition of Mercury's heavily cratered terrains. Additionally, we use mercurian cratering statistics (Fassett et al., 2011, 2012) to show that this new dynamical model of the early sculpting of the asteroid belt is supported by Mercury's cratering record.

2. Mercury's impactor population

The source for the LHB impactors is likely the primordial main asteroid belt, but early works had difficulty explaining why so many asteroids would hit the terrestrial planets a few hundred million years after the endpoint of planet formation (Strom et al., 2005). The Nice Model for early Solar System evolution suggests the increase in impact rate associated with the LHB occurred when Jupiter and Saturn cross a 1:2 mean motion resonance, scattering cometary and asteroidal material onto the planets (Gomes et al., 2005; Tsiganis et al., 2005).

A recent re-evaluation of the number and ages of lunar basins and the number and ages of terrestrial impact spherule beds, which are a product of the vaporized rock during an impact, suggests that objects may have hit the planets over a longer period of time than previously thought (Simonson and Glass, 2004; Hassler et al., 2011; Bottke et al., 2012). The additional impactors are thought to come from the so-called "E-belt", which is an extension of the asteroid belt that was located interior to the present-day belt. This extended belt is now extinct, but the Hungaria asteroid family is thought to harbor its few survivors (Warner et al., 2009; Bottke et al., 2012; Morbidelli et al., 2012). Orbital integrations seeking to study the effect of giant planet migration on the evolution of an extended asteroid belt (Gomes et al., 2005; Tsiganis et al., 2005; Bottke et al., 2012) show the terrestrial planets' bombardment occurred primarily in two stages: (i) a pre-LHB consisting of remnant planetesimals in the inner Solar System and E-belt projectiles sent into planet-crossing trajectories via gravitational interactions with Mars, and (ii) the LHB, triggered by giant planet migration during which the main belt and E-belt are excited to higher impact velocities when resonances with the giant planets sweep across the primordial asteroid belt. These simulations indicate the E-belt is the principal source of LHB impactors (Bottke et al., 2007, 2012; Morbidelli et al., 2012). Using a similar approach to Bottke et al. (2012) and our own Monte Carlo methods, we show that Mercury's cratering record supports this new model.

2.1. Methods

The Size-Frequency Distribution (SFD) of the E-belt is equivalent to the main belt because it was merely its extension (Bottke et al., 2012); therefore, we use the present-day asteroid belt SFD, which is derived from absolute magnitude data (Ivezić et al., 2001; Jedicke et al., 2002) and converted to projectile diameter D (km) = $1329\rho_v^{-\frac{1}{2}}10^{-H/5}$, where $\rho_v = 0.092$ is the visual geometric albedo,

and H is the absolute magnitude (Bottke et al., 2005b; Fowler and Chillemi, 1992). The present-day asteroid belt SFD is used because dynamical simulations suggest the asteroid belt quickly evolves to its present-day structure (Bottke et al., 2005a). The distribution has two major slope breaks: one near projectile diameter $D \sim 3$ to 4 km and another for $D \sim 100$ km (Bottke et al., 2005b). Owing to the resolution of our 3-D model (see Section 3), we consider projectiles with $D \geq 5$ km. Thus, our SFD contains only one major inflection point following a differential power law in mass (m) of the form $dN/dm \propto m^{-1.7}$ for $D \leq 100$ km and $dN/dm \propto m^{-2.2}$ for $D \geq 100$ km (Jedicke et al., 2002; Bottke et al., 2005b), assuming an impactor density $\rho_i = 2.7$ g/cm³ (Ivanov et al., 2002; Bottke et al., 2005b, 2012; Le Feuvre and Wieczorek, 2011), which is similar to CM meteorites (Britt et al., 2002).

Impactor masses are randomly selected to create a distribution consistent with the primordial main belt SFD. We constrain the total mass of objects impacting Mercury by the mass hitting the Moon and the relative impact probabilities between the two bodies. The total mass accreted by the Moon during its bombardment history, which is derived from isotopic studies of lunar mantle melts (Walker et al., 2004; Day et al., 2007, 2010), has been estimated to be $\sim 3.5 \times 10^{22}$ g (Morbidelli et al., 2012). Crater densities in the Nectaris basin suggest a total mass of $\sim 2 \times 10^{21}$ g has bombarded the Moon since 4.1 Gya (Morbidelli et al., 2012); thus, $\sim 3.3 \times 10^{22}$ g of asteroidal material impacts the Moon during the pre-LHB. Dynamical studies indicate mean pre-LHB and LHB lunar impact velocities of 11.9 km/s and 20.7 km/s respectively (Bottke et al., 2012). Le Feuvre and Wieczorek (2011) estimate the ratio between the impact probabilities on the Moon and Mercury to be 1.82, and suggest that mean impact velocities on Mercury should be a factor of 2.16 higher than the Moon. These ratios along with the approximations to the total lunar bombarding mass suggest Mercury has accreted $\sim 6.4 \times 10^{22}$ g during its bombardment history; 6×10^{22} g in the pre-LHB and 4×10^{21} g in the LHB. The mean impact velocity in the pre-LHB is 25.7 km/s and in the LHB is 44.7 km/s.

Assuming the density of Mercury's outer layer is $\rho_m = 3.7$ g/cm³ (Smith et al., 2012), Pi scaling laws suggest a projectile of diameter D impacting at velocity v_i produces a transient crater of diameter (Ivanov et al., 2002)

$$D_{tc} = 1.16 \left(\frac{\rho_i}{\rho_m} \right)^{\frac{1}{3}} D^{0.78} (v_i \sin \Omega)^{0.43} g^{-0.22}, \quad (1)$$

where $g = 3.7$ m/s² is Mercury's gravity, and Ω is the impact angle, the distribution of which follows $d\Omega = \sin(2\Omega)$ such that 45° is the most common value. To account for the effect of impact angle on D_{tc} , we use the equivalent vertical projectile scaling, $D_{eq} = 1.07D(\sin \Omega)^{1/2}$ for $\Omega < 60^\circ$ and $D_{eq} = 1$ for $\Omega > 60^\circ$ (Pierazzo and Melosh, 2000; Barr and Canup, 2010). Both phases of the bombardment history are simulated assuming impact velocities follow a Rayleigh distribution about the mean values for the pre-LHB and LHB. The synthetic transient crater population is converted to their final crater diameter following

$$D_{fc} = 1.17 \left(\frac{D_{tc}^{1.13}}{D_x^{0.13}} \right), \quad (2)$$

where D_x is the crater diameter at which cratering shifts from the simple to complex regime (McKinnon and Schenk, 1985; Collins et al., 2005), which for Mercury has been found to range from 10–16 km (Pike, 1980, 1988), with current measurements indicating 12 km (Barnouin et al., 2012).

2.2. Results

The Monte Carlo bombardment model creates five hundred synthetic impactor populations and the average number and sizes

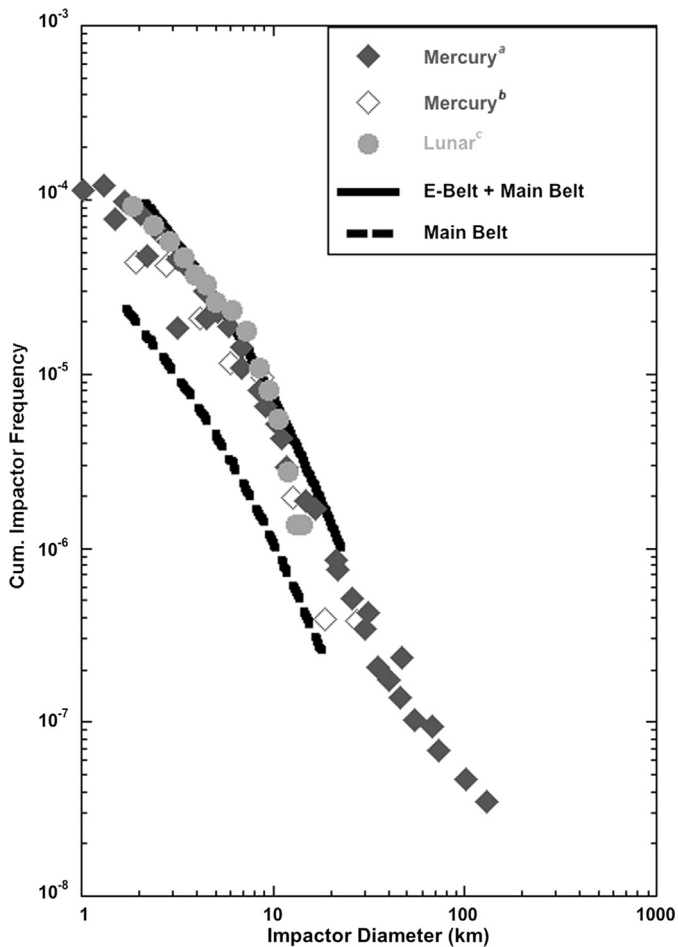


Fig. 1. Cumulative impactor size–frequency distribution estimated by converting the mercurian crater statistics from (a) Fassett et al. (2011) (filled diamonds), (b) Strom and Neukum (1988) (open diamonds), and the Moon from (c) Bottke et al. (2012) (circles) compared to the E-belt dominated (line) and pure main belt (dashed line) populations from Bottke et al. (2012).

of craters are compared to the global mercurian $N(D_{fc})$ values from Fassett et al. (2011, 2012), where N is the number of craters with diameters greater than D_{fc} per 10^6 km². We compare $N(20)$, $N(300)$, $N(500)$, and $N(1000)$. Our synthetic crater population produces $N(1000) = 0.04 \pm 0.02$ and $N(500) = 0.36 \pm 0.09$, which matches, within error, the observed values on Mercury of $N(1000) = 0.03 \pm 0.02$ and $N(500) = 0.23 \pm 0.05$; however, synthetic crater densities for $N(300)$ and $N(20)$ are higher than observed. Our model suggests $N(300) = 1.28 \pm 0.34$ and $N(20) = 220.73 \pm 62.14$ compared to observed global average values of $N(300) = 0.61 \pm 0.09$ and $N(20) = 94.38 \pm 1.35$. This difference may be due to resurfacing processes such as emplacement of smooth plains, which cover $\sim 27\%$ of Mercury's surface (Denevi et al., 2013), and resurfacing from intercrater plains. Indeed, the most densely cratered terrains on Mercury have regional $N(20) \sim 180$ (Fassett et al., 2011), which matches, within error, our synthetic crater population. The fact the observed $N(20)$ for the heavily cratered terrain on Mercury best matches the lower bound estimate may suggest *global* resurfacing, in agreement with Marchi et al. (2013). The close agreement among the mercurian N values and our simulations suggest the impacting population originated from the main belt and supports an E-belt dominated bombardment.

Additionally, using Eqs. (1) and (2) to convert crater size to impactor size, we show the E-belt size–frequency distribution matches the SFD of objects striking the mercurian heavily cratered terrains (Strom and Neukum, 1988; Strom et al., 2008;

Fassett et al., 2011). Fig. 1 compares a purely main belt derived population and an E-belt-dominated population (Bottke et al., 2012) against the inferred mercurian SFD. A Student's t -test indicates that to a 95% confidence, the E-belt-dominated population most closely matches the estimated mercurian population from cratering statistics.

Our results indicate the mercurian impactor population likely originates from the extended primordial asteroid belt, consistent with the dynamical scenario proposed by Bottke et al. (2012). Because the Moon's cratering record also supports an E-belt dominated bombardment (Bottke et al., 2012), our results indicate Mercury and the Moon had a similar impactor population, in support of previous work based on studying the shape of the lunar and mercurian crater SFD (Strom et al., 2005, 2008; Fassett et al., 2011). Additionally, the similarity between our synthetic crater population and observed cratering statistics suggest our approximated total impacting mass onto Mercury, which was scaled from lunar values, is reasonable. We note that in these simulations we do not account for post-LHB impactors, which are primarily derived from near-earth asteroids (Strom et al., 2005, 2011); however, most of the bombarding mass is accreted during the pre-LHB and LHB phase.

3. Impact-induced mixing

Impacts onto solid planetary bodies excavate, eject, and re-deposit material from depth into a continuous ejecta blanket where it is mixed with local material via ballistic sedimentation (Oberbeck, 1975; Melosh, 1989; Osinski et al., 2011). If there is a compositional difference between the surface and subsurface material, impacts will produce surface compositional heterogeneities that may be used to infer primordial structure. Here we model the effects of an E-belt dominated bombardment on the exhumation of material onto the surface using analytical and numerical techniques.

3.1. Analytic approach

Consider a body with its silicate layers divided into a crust of thickness δ_t that lies atop a mantle of differing composition (see Fig. 2). An impactor of diameter D , velocity v_i , and density ρ_i creates a transient crater of diameter D_{tc} . The Maxwell Z-Model suggests material ejected and deposited in the continuous ejecta blanket originates from a maximum depth of $(D_{tc}/2) \times (Z-2)(Z-1)^{(1-Z)/(Z-2)}$, with $Z=3$ giving a good match to experimental data, yielding a maximum of $D_{tc}/8$ (Maxwell, 1977; Austin et al., 1981; Melosh, 1989). Approximating the excavated volume as a hemisphere of an oblate spheroid, the total ejected volume is

$$V_{exc} = \frac{1}{48} \pi D_{tc}^3 \quad (3)$$

(Grieve and Garvin, 1984; Croft, 1985; Melosh, 1989; Garvin, 2000). If the impact punctures the crust (i.e., $D_{tc}/8 > \delta_t$), then the total excavated volume can be expressed as $V_{exc} = V_{ex/t} + V_{ex/m}$, where $V_{ex/t}$ is the component of the excavated volume originating from the crust, which can be approximated as a section of a spherical cap,

$$V_{ex/t} = V_{exc} \left[12 \frac{\delta_t}{D_{tc}} - 256 \left(\frac{\delta_t}{D_{tc}} \right)^3 \right], \quad (4)$$

and $V_{ex/m}$ is the volume of the excavated material sourced from the mantle. Assuming all of the excavated material is redeposited into the ejecta blanket and that ejected material is a homogeneous mixture of ejected crust and mantle, the volume fraction of mantle material within the continuous ejecta blanket is

$$\phi_m = 1 - \left(\frac{V_{ex/t}}{V_{exc}} \right), \quad (5)$$

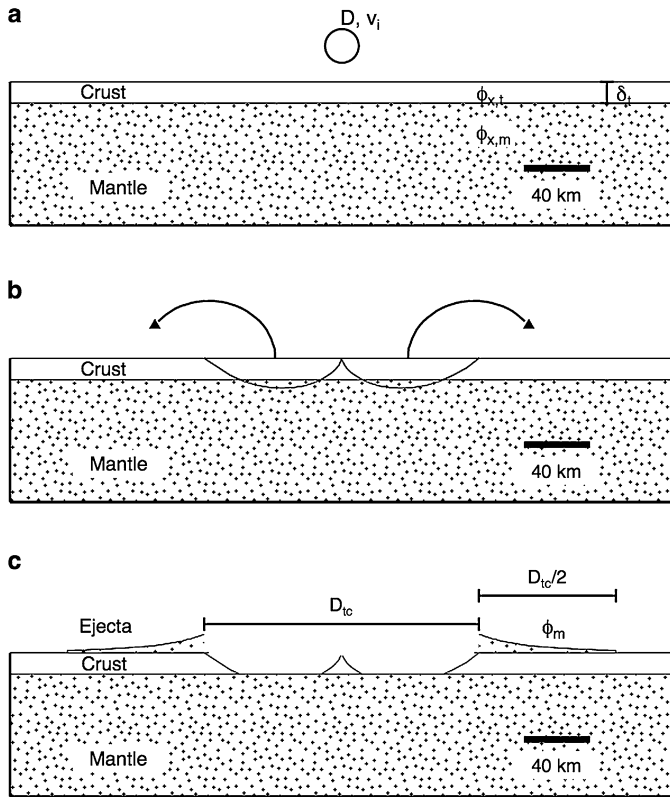


Fig. 2. (a) Schematic diagram of an impact of a $D = 20$ km projectile onto the crust (white) and mantle (black dots) of Mercury at $v_i = 30$ km/s, midway between the velocities appropriate for the LHB and pre-LHB, where δ_t is the crustal thickness, $\phi_{x,t}$ and $\phi_{x,m}$ are the volume fractions for a given element x within the crust and mantle respectively. (b) Material in the excavated region (solid bowls), which extends to a depth $D_{tc}/8$, is (c) redeposited into the continuous ejecta blanket (dotted regions on the surface), which extends $D_{tc}/2$ from the crater rim. We do not report the composition of material in crater floors (which, here show exposed mantle) because it is likely that landslides and other mass-wasting processes will modify crater floor compositions post-impact. The figure is mathematically to scale following the Maxwell-Z model for excavation with $Z = 3$.

where we define $\phi_m = 0$ for $V_{exc} \leq V_{ex/t}$. By construction, ϕ_m is also an upper bound estimate on the volumetric probability of finding mantle material within the ejecta blanket. Eq. (5) predicts that all craters with $D_{tc}/8 > \delta_t$ will become enriched in mantle material and that as craters become large, ejected material will be increasingly mantle-rich until the crustal component becomes negligible (i.e., $\lim_{D_{tc} \rightarrow \infty} (\phi_m) = 1$). Considering Caloris, the largest known mercurian impact basin ($D_{fc} \sim 1550$ km and $D_{tc} \sim 770$ km), Eq. (5) predicts $\phi_m \sim 0.29$, assuming $\delta_t = 50$ km. This represents the largest volume fraction of mantle material expected on the surface. Because the average crustal thickness on Mercury is estimated to be ~ 50 km (Smith et al., 2012), craters with transient diameters > 400 km ($D_{fc} \sim 740$ km) should puncture through the crust. Most impactors during Mercury's bombardment are thus expected to only excavate crustal material.

3.2. Monte Carlo cratering model

Our analytic approach suggests that surface enhancement in mantle material will primarily occur for basin-forming impacts, which are rare: $N(1000) = 0.03$ (see Section 2). Therefore, impact-induced mixing on the surface should be limited; however, as repeated impacts modify the crust, they will redistribute previously ejected mantle-rich material around basins across the surface. The distribution of mantle material in the outer tens of km of the crust will become heterogenous. Additionally, repeated impacts are expected to weaken the correlation between crater diameter and ϕ_m

because smaller impactors can excavate basin ejecta that is rich in mantle material. To understand the effect of repeated impacts, we develop a 3-D Monte Carlo model that tracks impact-induced compositional changes (Rivera-Valentin and Barr, 2014).

Mercury is modeled as a Cartesian sphere of radius 2440 km (Smith et al., 2012; Hauck et al., 2013) discretized into cubic volume elements 10 km on a side (Barr and Canup, 2010). Smith et al. (2012) adopted an average mercurian crustal thickness of 50 km and modeled Mercury's crust to vary in thickness from 20 to 80 km. Consequently, crustal thickness (δ_t) is considered a free parameter in our simulations. Initially, the probability of finding mantle material within the crust is zero while within the mantle it's 100% (i.e., $\phi_m = 0$ from the surface to the investigated crustal thickness while for the rest of the sphere $\phi_m = 1$).

Projectiles impacting the Cartesian sphere are chosen using Monte Carlo methods to follow the main belt SFD (see Section 2.1). A total of 6×10^{22} g of pre-LHB impactors arrive with an average velocity of 25.7 km/s followed by 4×10^{21} g of LHB impactors arriving at an average velocity of 44.7 km/s (Le Feuvre and Wieczorek, 2011; Bottke et al., 2012; Morbidelli et al., 2012). As in Section 2, impact velocities are Rayleigh distributed and impact angles follow $d\Omega = \sin(2\Omega)$, which is taken into account using the equivalent vertical projectile scaling. Impact location is selected by randomly picking a value for longitude within the range of 0° – 360° . Latitude values are distributed as $d\varphi = \sin(2\varphi)$ with most impacts occurring near the equator and fewer at the poles.

Once projectile properties are selected, the size of the transient crater is calculated from Eq. (1). Due to model resolution, the minimum transient crater considered is 10 km in diameter. This is not expected to drastically alter the final outcome because Eq. (5) suggests small craters will not cause significant impact-induced compositional variations. Resolution testing with elements of 5, 15, and 20 km on a side yield results that are within statistical error of those with an element size of 10 km. Because the transitional strength-to-gravity crater diameter on Mercury is 12 km (Barnouin et al., 2012), all simulated craters are assumed to be in the regime where excavation flow is controlled by gravity rather than strength.

The Maxwell Z-Model (Maxwell, 1977; Austin et al., 1981; Melosh, 1989) is used to define the excavation zone (Fig. 2). Thus, the excavated volume is approximated by an oblate spheroid of depth $D_{tc}/8$ and diameter D_{tc} . Excavated material from the spheroid is compositionally homogenized and redeposited on the surface in an annulus within a radial distance of D_{tc} from the impact point as depicted in Fig. 2. We only track the composition of ejecta blankets, not crater floors, because we consider it likely that mass-wasting processes will modify crater floor compositions post-impact (Osinski et al., 2011). Though generally the continuous ejecta blanket lies within $\sim D_{tc}$ from the impact point (Housen et al., 1983; McKinnon and Schenk, 1985; Housen and Holsapple, 2011), smaller blankets have been reported for Mercury (Gault et al., 1975). This is likely because Mercury's higher gravity creates a more confined ejecta blanket (McKinnon and Schenk, 1985) and so after crater modification, more of the blanket will lie within the final crater rim. In this work, we assume the continuous ejecta blanket lies within an annulus extending one crater radius away from the crater rim.

3.2.1. Results

Fig. 3 shows a sample post-bombardment map of the volume fraction of mantle material (ϕ_m) on the surface of a model mercury with a crustal thickness of $\delta_t = 50$ km. This simulated bombardment contained a single Caloris-sized crater at 0° latitude 83° longitude with $D_{tc} \sim 735$ km. Caloris-type impacts were only produced in $\sim 50\%$ of our simulations. The surface abundance of mantle material is quite heterogeneous despite the homogeneous crustal composition pre-bombardment. Mantle material is

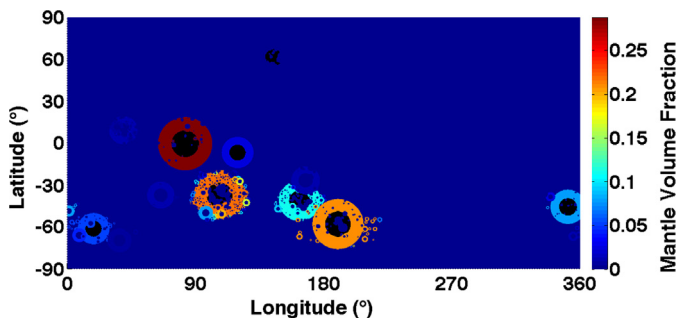


Fig. 3. Map of an example of the simulated post-bombardment volume fraction of mantle material within ejecta blankets (ϕ_m) for a Mercury with crustal thickness of 50 km. Black denotes crater floors, where mass-wasting, not included in our model, will likely modify surface composition. The color bar shows the magnitude of ϕ_m within ejecta blankets. (For interpretation of the references to color in this figure legend, the reader is referred to the web version of this article.)

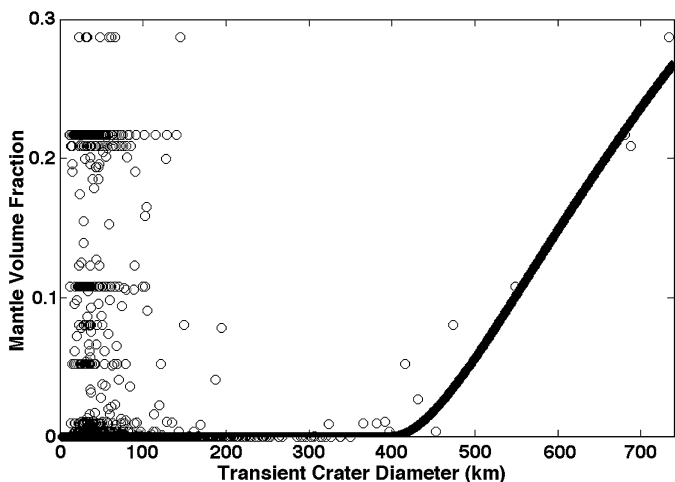


Fig. 4. Scatter plot of the mantle volume fraction (ϕ_m) within the continuous ejecta blanket for all craters in the Monte Carlo run illustrated in Fig. 3 as a function of transient crater diameter (open circles). The dashed line shows our analytical function (Eq. 5). For this simulation, $\delta_t = 50$ km, and only craters with $D_{tc} > 400$ km pierce through the crust.

regionally localized near large basins with $D_{tc}/8 > \delta_t$, but is not strictly limited to the ejecta blankets of large craters. Many small craters were able to excavate mantle-rich basin material and redistribute it away from the basin source.

In Fig. 4, the volume fraction of mantle material in the ejecta blankets of all craters in this simulation are plotted as a function of transient crater diameter. We also plot a line corresponding to our analytical model from Eq. (5). Though a relationship should exist between crater size and ejecta ϕ_m , overlapping impacts disrupt the function, creating only a weak association. Deviation from the analytic model for small craters with $D_{tc}/8 \leq \delta_t$ is caused by impactors that excavate mantle-rich material from basin ejecta. Similarly, deviation for craters with $D_{tc}/8 > \delta_t$ is caused when a large impactor is incident on or near a pre-existing basin with an enriched ejecta blanket. For this simulation, the average post-bombardment surface $\phi_m \sim 1\%$ with a maximum of $\sim 29\%$, within the ejecta around the Caloris-like impact crater.

Because the crustal thickness on Mercury is suggested to vary between $20 \text{ km} \leq \delta_t \leq 80 \text{ km}$ with an average value of 50 km (Smith et al., 2012), we conducted a suite of Monte Carlo simulations varying δ_t in increments of 20 km from 20 km to 100 km, including $\delta_t = 50$ km, and 125 km. The largest uncertainty from the modeled mercurian crustal thicknesses stem from the adopted average crustal thickness of 50 km (Smith et al., 2012); thus, we expand our crustal thickness range to include $\delta_t = 100$ km and

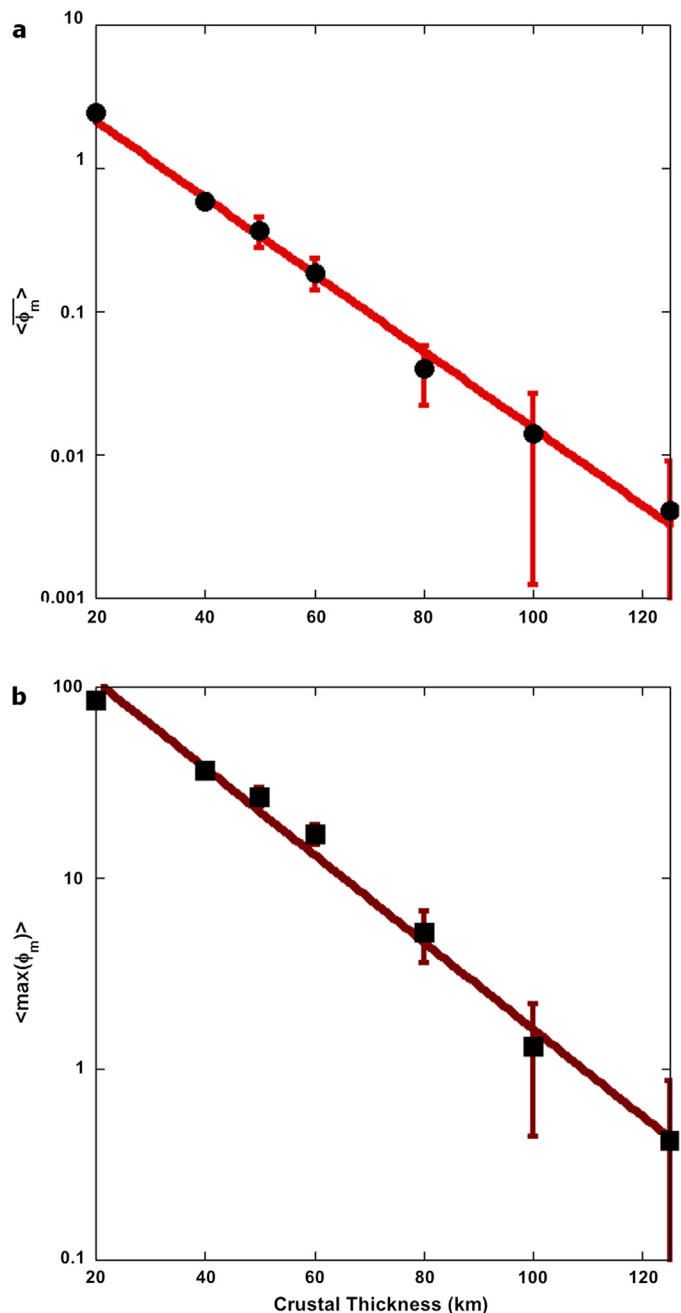


Fig. 5. The effect of impact mixing on the post-bombardment mantle abundance with respect to crustal thickness. Plotted values are the average from the Monte Carlo ensemble with their corresponding Monte Carlo error to a 95% confidence. (a) The volume fraction of mantle material averaged over the globe on the surface (circles). (b) The maximum volume fraction of mantle material within ejecta blankets (squares). Lines are the best fit function to Monte Carlo results. The y-axis is in log scale. Mantle volume fraction is shown in percent.

125 km. Two quantities are used to describe the heterogeneous post-bombardment distribution. For every Monte Carlo simulation, we record the average ($\overline{\phi_m}$) and the maximum ($\max(\phi_m)$) mantle volume fraction within ejecta blankets. For each δ_t explored, 100 bombardment histories are run such that the standard error for the reported means is within a 95% confidence interval of $\pm 25\%$. The average of the explored quantities over the 100 Monte Carlo runs is shown in Fig. 5, which plots the average post-bombardment ($\overline{\phi_m}$) and maximum ($\max(\phi_m)$) mantle volume fraction within ejecta blankets in percent, where the brackets denote the average over the Monte Carlo ensemble. Both quantities

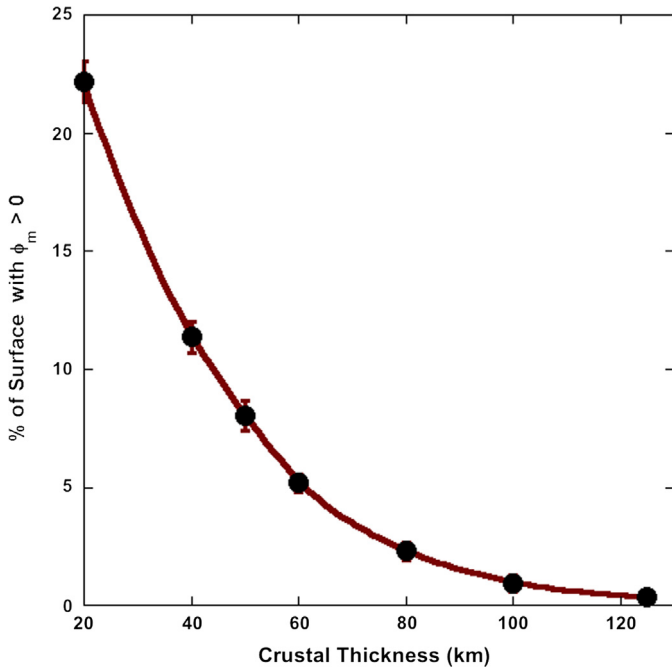


Fig. 6. The regional extent of impact-induced modification as a function of crustal thickness or depth to subsurface source. The y-axis represents the percent of the surface that is enriched in mantle material post-bombardment.

show a roughly power-law dependence with crustal thickness and approach zero for $\delta_t \geq 60$ km, at which point Mercury's bombardment does not excavate much mantle material. For a model mercury with a thin crust, $\delta_t = 20$ km, $\langle \overline{\phi_m} \rangle = 2.5\% \pm 0.1\%$ and $\langle \max(\phi_m) \rangle = 85.1\% \pm 3.4\%$. This quickly drops off after $\delta_t = 60$ km, where $\langle \overline{\phi_m} \rangle = 0.2\% \pm 0.05\%$ and $\langle \max(\phi_m) \rangle = 17\% \pm 2.1\%$. For the estimated average mercurian crustal thickness ($\delta_t = 50$ km), the ensemble average and maximum ϕ_m are $0.4\% \pm 0.09\%$ and $26.6\% \pm 3\%$ respectively.

Though on average the abundance of mantle material on the surface is low, ϕ_m is strongly enhanced in basin ejecta and overlapping impacts, significantly altering the regional composition as seen in Fig. 3. The size of the regional effect is dependent on the crustal thickness because thinner crusts permit more impactors to excavate through to the mantle. This process is shown in Fig. 6 and roughly follows a power law such that for $\delta_t \geq 100$ km, less than 1% of the surface contains mantle material. For a model Mercury with $\delta_t = 50$ km, on average, $8.0\% \pm 3.2\%$ of the area on the surface is enriched with mantle material. The enrichment varies between $\sim 0.2\%$ and 22% and is inversely proportional to crustal thickness. Although some locations remain unaffected by impactors with $D \geq 5$ km, on average, each 10×10 km element on the surface is covered 1.1 ± 0.3 times by an ejecta blanket and is disrupted by a crater bowl 0.4 ± 0.1 times.

4. Discussion

4.1. Implications for the origin of LRM

Considering our model results for relating crustal thickness to surface spatial coverage of mantle material (Fig. 6), we can estimate the depth to the LRM's darkening agent. Here, the "crustal thickness" can be considered as a proxy for the depth to the subsurface source. Our Monte Carlo simulations suggest that in order to produce the $\sim 15\%$ surface coverage of LRM, the depth to the source region should be 30 ± 5 km, the error arises from the Monte Carlo methods. Because the crustal thickness on Mercury is modeled to vary between 20 and 80 km with an average of 50 km

(Smith et al., 2012), this implies the darkening agent source is most probably located within a chemically distinct lower crust.

Additionally, if the darkening agent for the LRM comes from depth, our model reproduces the weak association between crater size and LRM abundance (e.g., Fig. 5). In our model, this weak association is produced by repeated and overlapping impacts. Thus, our results suggest that subsurface heterogeneity is not required to produce the weak association between crater size and LRM abundance within crater ejecta.

4.2. Implications for impact-induced chemical variations

If the mercurian crust has a chemically distinct lower crust, i.e., enriched or depleted in a given element, then impact excavation of subsurface material will alter the composition of the outer few kilometers of the crust. Revisiting Eq. (5), the volume fraction for a given element x within an ejecta blanket produced by an impact that has excavated through to the chemically distinct lower crust is

$$\phi_{x,ejb} = \phi_{x,t}(1 - \phi_m) + \phi_{x,m}(\phi_m), \quad (6)$$

where $\phi_{x,t}$ and $\phi_{x,m}$ are the volume fractions of element x in the crust and subsurface respectively (see Fig. 2). This formulation can aid in determining the ancient, LHB-era surface–subsurface compositional difference by observing the highest/lowest surface abundance of a given element within ejecta blankets.

In a simple, linear, interpretation of the effect of LRM on reflectance, the 30% reduction in reflectance could indicate that $\phi_{x,ejb} = 0.3$. From Section 4.1, we estimate the darkening agent's source is ~ 30 km deep. From Fig. 5b, the largest volume fraction of material from this depth on the surface is $\phi_m \sim 0.63$. Then, assuming initially the surface volume fraction of the darkening agent is zero (i.e., $\phi_{x,ejb} = \phi_{x,m}\phi_m$), in order to reproduce the maximum 30% volume fraction of darkening agent, $\phi_{x,m} \sim 48\%$. This serves as a first order approximation to the compositional difference between the upper and the chemically distinct lower crust.

To generalize, consider the case where $\phi_{x,m} = f\phi_{x,t}$, where f is the enhancement factor indicating the enrichment or depletion of element x in the chemically distinct lower crust with respect to the surface. Then, the volume fraction of element x in the ejecta blanket can be written as $\phi_{x,ejb} = \xi\phi_{x,t}$, where

$$\xi = 1 + \phi_m(f - 1). \quad (7)$$

This shows the post-bombardment compositional enhancement or depletion from impact-induced mixing is less pronounced than the compositional difference between the lower crust and surface. When the lower crust is enriched relative to the surface (i.e., $f > 1$), $\xi < f$ so that a strong subsurface enrichment only slightly enriches the surface. Additionally, when the lower crust is depleted in element x with respect to the surface (i.e., $f < 1$), $\xi > f$ so that a strong subsurface depletion only slightly reduces the observed composition post-bombardment. Thus, the post-bombardment enrichment or depletion on the surface will be less than the ancient compositional difference between the chemically distinct lower crust and surface when $\phi_m < 1$.

Applying our Monte Carlo results for the expected maximum surface volume fraction of mantle material (Fig. 5b), using crustal thickness as a proxy for the depth to the chemically distinct lower crust, and studying an enhancement factor of $0 \leq f \leq 5$, we plot the expected ξ in Fig. 7. As can be seen, there are two "lobes" on either end of the y-axis separated at $f = 1$ and a zone where $\xi \sim 1$. This zone, where relative post-bombardment enhancement/depletion on the surface is negligible, encompasses a larger swath of f values for thicker crustal thicknesses. Thus, the

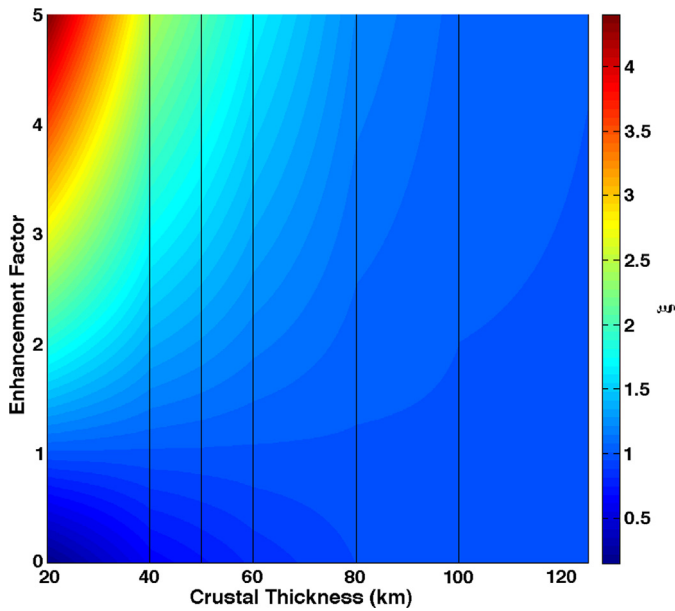


Fig. 7. Surface ejecta enhancement factor (ξ , see Eq. (7)) for the largest craters as a function of crustal thickness and mantle/crust enhancement factor (f). Color mapping is interpolated between our Monte Carlo results, which are along the vertical lines and the endpoints. Deviations from a smooth trend, as can be seen around 100 km, are due to Monte Carlo methods. (For interpretation of the references to color in this figure legend, the reader is referred to the web version of this article.)

thicker the crust, the more difficult it is to observe the surface–lower crust compositional difference even if it is severe. For thin crusts (i.e., $\delta_t \leq 60$ km), the surface–lower crust compositional difference is more apparent. For example, considering $\delta_t = 20$ km and $f = 5$, $\xi = 4.4$ and so the surface–lower crust compositional difference is only diluted by $\sim 12\%$. In general, for $\delta_t > 80$ km surface–lower crust depletion will not be apparent on the surface while enhancement will only be significantly apparent for strong compositional differences.

As can be seen in Fig. 4, though, not all the ejecta composition of large craters will follow this simple analytical model. That is because the composition of the ejecta blanket is not only dependent on the geometry of the excavation process, but also the surface history. If an impactor excavates material from an area that was previously enriched in subsurface material, its ejecta blanket will be further enriched. The end-member ejecta blanket composition of many large craters are a product of modification by smaller impacts. The general effect of these smaller overlapping impacts is to lower the overall magnitude of enrichment surrounding the basin because their composition will largely be crustal in origin. Thus, the maximum abundance of subsurface material within an ejecta blanket will be a lower bound estimate on the surface–subsurface compositional difference (f).

Additionally, Mercury is suggested to have been globally modified by volcanism that may have been concurrent with the LHB (Head et al., 2008; Strom et al., 2011; Marchi et al., 2013). This would serve to further modify the composition of the surface and introduce chemical heterogeneity. Our work, though, focuses on impact-induced surface chemical heterogeneity, and thus provides an approximation to subsurface structure and composition.

5. Conclusions

The recent reevaluation of the early history of the inner Solar System suggests the primordial asteroid belt could have originally extended well into the Mars-crossing zone (Bottke et al., 2012; Morbidelli et al., 2012). The extended region, termed the E-belt, would have provided the majority of projectiles during the period

of frequent impacts beginning ~ 4.1 Gya, the Late Heavy Bombardment (Hartmann et al., 2000; Bottke et al., 2012). Here, we show that the predicted two-stage E-belt dominated bombardment is consistent with the mercurian spatial crater densities. Consequently, both Mercury and the Moon shared the same impactor population, which is also supported by the similarity in the shape of their respective crater size–frequency distributions. Because our Monte Carlo results correlate well with observed spatial crater densities, the estimated bombardment mass is consistent with estimated masses for the E-belt.

Mercury's crustal thickness is suggested to be between 20 and 80 km with an average of 50 km (Smith et al., 2012); therefore, impacts into Mercury's thin crust should have a significant effect on surface composition by excavation and redistribution of mantle material. Here, we develop a Monte Carlo model of impact cratering, excavation, and ejecta blanket deposition along with analytical methods, to show that the mercurian bombardment produces a heterogeneous post-bombardment surface composition from an initially homogeneous crust and mantle. Though the global volumetric abundance of mantle material excavated on the surface is low, mantle-enriched material is strongly concentrated in basin ejecta because those large events pierce through the crust. Overlapping and repeated impacts serve to redistribute material away from their basin source. The extent of the regional mixing is shown to be strongly controlled by crustal thickness because thin crusts allow for easier excavation of mantle material. Considering a model mercury with a crustal thickness of 50 km, the volume fraction of mantle material averaged over the globe is $\sim 0.4\%$ with a maximum of $\sim 27\%$. Our results suggest that mantle-enriched material would cover about 8% of the surface for this case.

Furthermore, our results can be used to infer the source depth of the darkening agent responsible for the mercurian Low Reflectance Material. LRM is found within crater and basin ejecta, though not all ejecta contain LRM. This weak association with crater size and LRM abundance has been used to infer that the subsurface source for the darkening agent is heterogeneous (Denevi et al., 2009). We show that the association of LRM with ejecta deposits can be a consequence of the excavation of a darkening agent at depth and its subsequent deposition in ejecta blankets, and the weak association between reflectance and crater size may evolve, at least in part from, repeated and overlapping impacts. Our model suggests that in order to produce the nearly 15% surface coverage of LRM (Denevi et al., 2009), the source depth of the darkening agent may be ~ 30 km. Because the average mercurian crustal thickness is suggested to be 50 km (Smith et al., 2012), the darkening agent may originate from a chemically distinct lower crust.

Monte Carlo results along with our analytical methods suggest that if an ancient, LHB-era compositional difference exists between the mercurian upper and lower crust, there will be regions post-bombardment that will have compositions reflecting this difference. The post-bombardment compositional enhancement or depletion within a given crater from impact-induced mixing will be less pronounced than the upper crust–subsurface difference, but the ejecta blanket composition can be used to infer the magnitude of the compositional difference between the upper and lower crust. Assuming a direct relationship between reflectance and composition, we estimate the inferred chemically distinct lower crust contains $\sim 48\%$ darkening agent by volume in order to reproduce observations of $\sim 30\%$ reduction in reflectance. In general, given the spatial distribution of a given element that is associated with crater ejecta, our results allow the source depth to be estimated. Using this depth along with the abundance of the element in the largest crater's ejecta deposit, the crust–subsurface compositional difference pre-bombardment can be estimated.

Mercury's surface, though, has been heavily modified by volcanism that may have been active during parts of the LHB (Head et al., 2008; Strom et al., 2011; Marchi et al., 2013). *Wide-scale resurfacing, which may have worked concurrently with the LHB to add surface heterogeneity, is expected on Mercury, and so our results provide an approximation to subsurface composition and structure.* High-resolution regional compositional mapping from MESSENGER of the heavily cratered terrains can allow for inferences of the ancient subsurface composition given the spatial distribution of elements associated with crater ejecta and their relative surface abundance.

Acknowledgements

This work is supported through the Center for Lunar Origin and Evolution under the NASA Lunar Science Institute through NNA09DB32A and PG&G NNX12AI76G. The authors thank Brett Denevi and an anonymous reviewer who helped enhance this manuscript.

References

- Austin, M.G., Thomsen, J.M., Ruhl, S.F., Orphal, D.L., Borden, W.F., Larson, S.A., Schultz, P.H., 1981. Z-model analysis of impact cratering – An overview. In: Proceedings of the Conference on Multi-ring Basins: Formation and Evolution. Pergamon, pp. 197–205.
- Barnouin, O.S., Zuber, M.T., Smith, D.E., Neumann, G.A., Herrick, R.R., Chappelow, J.E., Murchie, S.L., Prockter, L.M., 2012. The morphology of craters on Mercury: Results from MESSENGER flybys. *Icarus* 219, 414–427.
- Barr, A.C., Canup, R.M., 2010. Origin of the Ganymede–Callisto dichotomy by impacts during the late heavy bombardment. *Nat. Geosci.* 3, 164–167.
- Bottke, W.F., Durda, D.D., Nesvorný, D., Jedicke, R., Morbidelli, A., Vokrouhlický, D., Levison, H., 2005a. The fossilized size distribution of the main asteroid belt. *Icarus* 175 (1), 111–140.
- Bottke, W.F., Durda, D.D., Nesvorný, D., Jedicke, R., Morbidelli, A., Vokrouhlický, D., Levison, H.F., 2005b. Linking the collisional history of the main asteroid belt to its dynamical excitation and depletion. *Icarus* 179, 63–94.
- Bottke, W.F., Levison, H.F., Nesvorný, D., Dones, L., 2007. Can planetesimals left over from terrestrial planet formation produce the lunar Late Heavy Bombardment?. *Icarus* 190, 203–223.
- Bottke, W.F., Vokrouhlický, D., Minton, D., Nesvorný, D., Morbidelli, A., Brasser, R., Simonson, B., Levison, H.F., 2012. An Archaean heavy bombardment from a destabilized extension of the asteroid belt. *Nature* 485, 78–81.
- Britt, D.T., Yeomans, D., Housen, K., Consolmagno, G., 2002. Asteroid density, porosity, and structure. In: Bottke, W.F., Cellino, A., Paolicchi, P., Binzel, R.P. (Eds.), *Asteroids III*. University of Arizona Press, pp. 485–500.
- Collins, G.S., Melosh, H.J., Marcus, R.A., 2005. Earth impact effects program: A web-based computer program for calculating the regional environmental consequences of a meteoroid impact on Earth. *Meteorit. Planet. Sci.* 40, 817–840.
- Croft, S.K., 1985. The scaling of complex craters. *J. Geophys. Res.* 15, 828–842.
- Day, J.M.D., Pearson, D.G., Taylor, L.A., 2007. Highly siderophile element constraints on accretion and differentiation of the Earth–Moon system. *Science* 315, 217–219.
- Day, J.M.D., Walker, R.J., James, O.B., Puchtel, I.S., 2010. Osmium isotope and highly siderophile element systematics of the lunar crust. *Earth Planet. Sci. Lett.* 289, 595–605.
- Denevi, B., Robinson, M., 2008. Mercury's albedo from Mariner 10: Implications for the presence of ferrous iron. *Icarus* 197, 239–246.
- Denevi, B.W., Robinson, M.S., Solomon, S.C., Murchie, S.L., Blewett, D.T., Domingue, D.L., McCoy, T.J., Ernst, C.M., Head, J.W., Watters, T.R., 2009. The evolution of Mercury's crust: A global perspective from MESSENGER. *Science* 324, 613–618.
- Denevi, B.W., Ernst, C.M., Meyer, H.M., Robinson, M.S., Murchie, S.L., Whitten, J.L., Head, J.W., Watters, T.R., Solomon, S.C., Ostrach, L.R., Chapman, C.R., Byrne, P.K., Klimczak, C., Peplowski, P.N., 2013. The distribution and origin of smooth plains on Mercury. *J. Geophys. Res., Planets* 118. <http://dx.doi.org/10.1002/jgre.20075>.
- Evans, L.G., Starr, R.D., Weider, S.Z., Boynton, W.V., Hamara, D.K., Goldsten, J.O., Peplowski, P.N., Rhodes, E., Lawrence, D.J., McCoy, T., Nittler, L., Solomon, S.C., Sprague, A.L., Stockstill-Cahill, K., 2012. Major-element abundances on the surface of Mercury: Results from the MESSENGER gamma-ray spectrometer. *J. Geophys. Res.* 117, E00L07.
- Fassett, C.I., Kadish, S.J., Head, J.W., Solomon, S.C., Strom, R.G., 2011. The global population of large craters on Mercury and comparison with the Moon. *Geophys. Res. Lett.* 38, L10202.
- Fassett, C.I., Head, J.W., Baker, D.M.H., Zuber, M.T., Smith, D.E., Neumann, G.A., Solomon, S.C., Klimczak, C., Strom, R.G., Chapman, C.R., Prockter, L.M., Phillips, R.J., Oberst, J., Preusker, F., 2012. Large impact basins on Mercury: Global distribution, characteristics, and modification history from MESSENGER orbital data. *J. Geophys. Res.* 117, E00L08.
- Fowler, J., Chillemi, J., 1992. IRAS asteroid data processing. In: *The IRAS Minor Planet Survey*. Phillips Laboratory, Hanscom AF Base, MA, pp. 17–43. Tech. Rep. PL-TR-92-2049.
- Garvin, J., 2000. North polar region craterforms on Mars: Geometric characteristics from the Mars orbiter laser altimeter. *Icarus* 144, 329–352.
- Gault, D.E., Guest, J.E., Murray, J.B., Dzurisin, D., Malin, M.C., 1975. Some comparisons of impact craters on Mercury and the Moon. *J. Geophys. Res.* 80, 2444–2460.
- Gomes, R., Levison, H.F., Tsiganis, K., Morbidelli, A., 2005. Origin of the cataclysmic Late Heavy Bombardment period of the terrestrial planets. *Nature* 435, 466–469.
- Grieve, R., Garvin, J.B., 1984. A geometric model for excavation and modification at terrestrial simple impact craters. *J. Geophys. Res.* 89, 11561–11572.
- Hartmann, W.K., Ryder, G., Dones, L., Grinspoon, D., 2000. The time-dependent intense bombardment of the primordial Earth/Moon system. In: Canup, R.M., Righter, K., 69 collaborating authors (Eds.), *Origin of the Earth and Moon*. University of Arizona Press, Tucson, pp. 493–512.
- Hassler, S.W., Simonson, B.W., Sumner, D.Y., Bodin, L., 2011. Paraburdoo spherule layer (Hamersley Basin, Western Australia): Distal ejecta from a fourth large impact near the Archaean–Proterozoic boundary. *Geology* 39, 307–310.
- Hauk II, S.A., Margot, J.-L., Solomon, S.C., Phillips, R.J., Johnson, C.L., Lemoine, F.G., Mazarico, E., McCoy, T.J., Padovan, S., Peale, S.J., Perry, M.E., Smith, D.E., Zuber, M.T., 2013. The curious state of Mercury's internal structure. *J. Geophys. Res., Planets* 118, 1–17.
- Head, J.W., Murchie, S.L., Prockter, L.M., Robinson, M.S., Solomon, S.C., Strom, R.G., Chapman, C.R., Watters, T.R., McClintock, W.E., Blewett, D.T., Gillis-Davis, J.J., 2008. Volcanism on Mercury: Evidence from the first MESSENGER flyby. *Science* 321, 69–72.
- Housen, K.R., Holsapple, K.A., 2011. Ejecta from impact craters. *Icarus* 211, 856–875.
- Housen, K.R., Schmidt, R.M., Holsapple, K.A., 1983. Crater ejecta scaling laws – Fundamental forms based on dimensional analysis. *J. Geophys. Res.* 88, 2485–2499.
- Ivanov, B.A., Neukum, G., Bottke, W.F., Hartmann, W.K., 2002. The comparison of size–frequency distributions of impact craters and asteroids and the planetary cratering rate. In: Bottke, W.F., Cellino, A., Paolicchi, P., Binzel, R.P. (Eds.), *Asteroids III*, vol. 1. University of Arizona Press, pp. 89–101.
- Ivezić, Ž., Tabachnik, S., Rafikov, R., Lupton, R.H., Quinn, T., Hammergren, M., Eyer, L., Chu, J., Armstrong, J.C., Fan, X., et al., CDSS Collaboration, 2001. Solar System objects observed in the Sloan Digital Sky Survey commissioning data. *Astron. J.* 122, 2749–2784.
- Jedicke, R., Larsen, J., Spahr, T., 2002. Observational selection effects in asteroid surveys and estimates of asteroid population sizes. In: Bottke, W.F., Cellino, A., Paolicchi, P., Binzel, R.P. (Eds.), *Asteroids III*. University of Arizona Press, pp. 71–87.
- Le Feuvre, M., Wiczorek, M.A., 2011. Nonuniform cratering of the Moon and a revised crater chronology of the inner Solar System. *Icarus* 214, 1–20.
- Marchi, S., Chapman, C.R., Fassett, C.I., Head, J.W., Bottke, W.F., Strom, R.G., 2013. Global resurfacing of Mercury 4.0–4.1 billion years ago by heavy bombardment and volcanism. *Nature* 499, 59–61.
- Maxwell, D.E., 1977. Simple Z model for cratering, ejection, and the overturned flap. In: *Impact and Explosion Cratering: Planetary and Terrestrial Implications*, Proceedings of the Symposium on Planetary Cratering Mechanics. Pergamon, pp. 1003–1008.
- McKinnon, W.B., Schenk, P.M., 1985. Ejecta blanket scaling on the Moon and inferences for projectile populations. In: *Lunar and Planetary Institute Science Conference Abstracts*, vol. 16, pp. 544–545.
- Melosh, H.J., 1989. *Impact Cratering: A Geologic Process*. Oxford University Press, New York.
- Morbidelli, A., Marchi, S., Bottke, W.F., Kring, D.A., 2012. A sawtooth-like timeline for the first billion years of lunar bombardment. *Earth Planet. Sci. Lett.* 355–356, 144–151.
- Murchie, S.L., Watters, T.R., Robinson, M.S., Head, J.W., Strom, R.G., Chapman, C.R., Solomon, S.C., McClintock, W.E., Prockter, L.M., Domingue, D.L., Blewett, D.T., 2008. Geology of the Caloris Basin, Mercury: A View from MESSENGER. *Science* 321, 73–76.
- Nittler, L.R., Starr, R.D., Weider, S.Z., McCoy, T.J., Boynton, W.V., Ebel, D.S., Ernst, C.M., Evans, L.G., Goldsten, J.O., Hamara, D.K., 2011. The major-element composition of Mercury's surface from MESSENGER X-ray spectrometry. *Science* 333, 1847–1850.
- Oberbeck, V.R., 1975. The role of ballistic erosion and sedimentation in lunar stratigraphy. *Rev. Geophys. Space Phys.* 13, 337–362.
- Osinski, G.R., Tornabene, L.L., Grieve, R.A.F., 2011. Impact ejecta emplacement on terrestrial planets. *Earth Planet. Sci. Lett.* 310, 167–181.
- Peplowski, P.N., Lawrence, D.J., Rhodes, E.A., Sprague, A.L., McCoy, T.J., Denevi, B.W., Evans, L.G., Head, J.W., Nittler, L.R., Solomon, S.C., Stockstill-Cahill, K.R., Weider, S.Z., 2012. Variations in the abundances of potassium and thorium on the surface of Mercury: Results from the MESSENGER gamma-ray spectrometer. *J. Geophys. Res.* 117, E00L04.
- Pierazzo, E., Melosh, H.J., 2000. Melt production in oblique impacts. *Icarus* 145, 252–261.
- Pike, R.J., 1980. Control of crater morphology by gravity and target type – Mars, Earth, Moon. In: *Proc. 11th Lunar Planet. Sci. Conf.*, pp. 2159–2189.

- Pike, R.J., 1988. Geomorphology of impact craters on Mercury. In: Vilas, F., Chapman, C.R., Mathews, M.S. (Eds.), Mercury, vol. 1. University of Arizona Press, pp. 165–273.
- Rivera-Valentin, E.G., Barr, A.C., 2014. Estimating the size of late veneer impactors from impact-induced mixing on Mercury. *Astrophys. J. Lett.* 782, L8.
- Robinson, M.S., Murchie, S.L., Blewett, D.T., Domingue, D.L., Hawkins, S.E., Head, J.W., Holsclaw, G.M., McClintock, W.E., McCoy, T.J., McNutt, R.L., Prockter, L.M., Solomon, S.C., Watters, T.R., 2008. Reflectance and color variations on Mercury: Regolith processes and compositional heterogeneity. *Science* 321, 66–69.
- Simonson, B.M., Glass, B.P., 2004. Spherule layers – records of ancient impacts. *Annu. Rev. Earth Planet. Sci.* 32, 329–361.
- Smith, D.E., Zuber, M.T., Phillips, R.J., Solomon, S.C., Hauck, S.A., Lemoine, F.G., Mazarico, E., Neumann, G.A., Peale, S.J., Margot, J.L., Johnson, C.L., Torrence, M.H., Perry, M.E., Rowlands, D.D., Goossens, S., Head, J.W., Taylor, A.H., 2012. Gravity field and internal structure of Mercury from MESSENGER. *Science* 336, 214–217.
- Strom, R.G., Neukum, G., 1988. The cratering record on Mercury and the origin of impacting objects. *Mercury*, 336–373.
- Strom, R.G., Malhotra, R., Ito, T., Yoshida, F., Kring, D.A., 2005. The origin of planetary impactors in the inner Solar System. *Science* 309 (5742), 1847–1850.
- Strom, R.G., Chapman, C.R., Merline, W.J., Solomon, S.C., Head, J.W., 2008. Mercury cratering record viewed from MESSENGER's first flyby. *Science* 321, 79–81.
- Strom, R.G., Banks, M.E., Chapman, C.R., Fassett, C.I., Forde, J.A., Head, J.W., Merline, W.J., Prockter, L.M., Solomon, S.C., 2011. Mercury crater statistics from MESSENGER flybys Implications for stratigraphy and resurfacing history. *Planet. Space Sci.* 59, 1960–1967.
- Tera, F., Papanastassiou, D.A., Wasserburg, G.J., 1974. Isotopic evidence for a terminal lunar cataclysm. *Earth Planet. Sci. Lett.* 22, 1–21.
- Tsiganis, K., Gomes, R., Morbidelli, A., Levison, H.F., 2005. Origin of the orbital architecture of the giant planets of the Solar System. *Nature* 435, 459–461.
- Walker, R.J., Horan, M.F., Shearer, C.K., Papike, J.J., 2004. Low abundance of highly siderophile elements in the lunar mantle: evidence for prolonged late accretion. *Earth Planet. Sci. Lett.* 224, 399–413.
- Warner, B.D., Harris, A.W., Vokrouhlický, D., Nesvorný, D., Bottke, W.F., 2009. Analysis of the Hungaria asteroid population. *Icarus* 204, 172–182.
- Weider, S.Z., Nittler, L.R., Starr, R.D., McCoy, T.J., Stockstill-Cahill, K.R., Byrne, P.K., Denevi, B.W., Head, J.W., Solomon, S.C., 2012. Chemical heterogeneity on Mercury's surface revealed by the MESSENGER X-ray spectrometer. *J. Geophys. Res.* 117, E00L05.